

Which Process Limits the Operation of a Li–S System?

Sara Drvarič Talian,^{†,‡} Gregor Kapun,[†] Jože Moškon,[†] Alen Vizintin,^{†,§} Anna Randon-Vitanova,[§] Robert Dominko,^{†,‡,§} and Miran Gabersček^{*,†,‡,§}

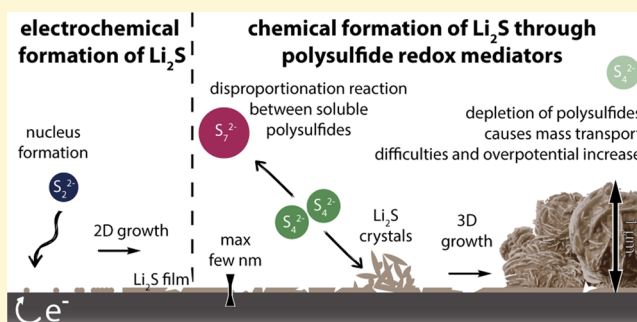
[†]Department of Materials Chemistry, National Institute of Chemistry, Hajdrihova 19, 1000 Ljubljana, Slovenia

[‡]Faculty of Chemistry and Chemical Technology, University of Ljubljana, Večna pot 113, 1000 Ljubljana, Slovenia

[§]Honda R&D Europe GmbH, Carl-Legien Strasse 30, 63703 Offenbach, Germany

Supporting Information

ABSTRACT: The impact of the solid film deposit (mainly Li_2S) on the complex electrochemistry of a Li–S cell is studied in detail. Already a simple, straightforward experiment strongly indicates that this impact might be much smaller than usually assumed. Notably, a similar phenomenon is demonstrated for another battery operated on the same basic principle: the magnesium–sulfur battery. In order to better detect the surface-specific phenomena associated with formation and properties of the solid surface deposit, we construct special electrochemical cells with a flat glassy carbon disc or other well-defined materials. Different model systems are prepared in which crucial variables such as the electrode configuration, separator type, and state of charge are varied in a systematic and controlled way. Electrochemical results are supplemented with data from microstructural analysis, in particular focused ion beam–scanning electron microscopy (FIB–SEM) imaging and X-ray diffraction analysis. We show that the growth of the surface film is more complex than generally assumed and that its defect-rich morphology hardly represents any obstacle for electrochemical reaction(s) to take place. Rather, the cell operation is limited by diffusional processes and depletion of polysulfide concentration in electrolyte. The new insight into the occurrence, properties, and especially the impact of solid film deposits on operation of the Li–S system is expected to have important implications for future design of Li–S practical cells.



1. INTRODUCTION

The Li–S battery seems to be one of the most promising candidates to replace the predominating lithium ion systems. Indeed, during the past decade we have witnessed remarkable improvements in practical energy density, rate performance, and cycling stability of Li–S battery cells.^{1–6} Quite surprisingly, several open questions regarding the very basic operation of this complex system however remain unanswered. One point of controversy has been the role of the final solid product of discharge, Li_2S , which gets deposited on the surface of the conductive substrate (usually a high-surface area carbon) where the main electrochemical reactions take place. [The authors acknowledge that the actual mechanism may also involve deposition of other sulfur species (such as Li_2S_2). However, for the present purposes we will denote any solid deposit formed as Li_2S .] The current mainstream view is that the Li_2S deposit is very compact and essentially nonconductive⁷ and thus severely impacts the operation of the Li–S cell. In fact, many recent reports assume that it is the Li_2S film that limits the capacity of the system during the discharge half-cycle.^{4,8–15}

A generally accepted mechanism of electrochemical Li_2S precipitation is through nucleation followed by a two-dimensional (2D) film-like coverage expanding by growth on

the three-phase boundary of the electrode surface, the already formed precipitate, and the electrolyte solution. Due to the nonconductive nature of the Li_2S deposit it is expected that such compact 2D coverage will eventually completely passivate (block) the covered parts of the electrode, thus preventing any further cathodic reaction.^{16,17} This hypothesis has also been applied in modeling of the discharge process¹⁸ and has initiated several studies involving organic or inorganic redox mediators in order to enable three-dimensional deposition of lithium sulfide which could in turn increase the obtained capacity.^{19–21}

There are, however, other studies that directly or indirectly contradict the assumption of the capacity limiting role of Li_2S . For example, a nonencapsulation approach for high-performance Li–S batteries²² has recently been published, where large (>1 μm) particles of Li_2S deposit are detected at the end of discharge, suggesting a growth significantly beyond the threshold thickness for electron tunneling (generally several nanometers for insulating films).²³ This extensive growth indicates that Li_2S is not necessarily deposited in a form of a

Received: August 12, 2019

Revised: October 13, 2019

Published: October 14, 2019

thin, quasi-2D compact passive layer, as suggested in previous works.¹⁶ Moreover, Waluś et al.¹⁴ also reported formation of a dense, 150–200 nm thick Li₂S layer which is between 1 and 2 orders of magnitude thicker than the maximum value allowed if the film was compact and nonconductive.²³ More indirectly, our previous study²⁴ demonstrated significant discharge capacities of special geometry Li–S battery cells where planar glassy carbon electrodes with merely 2 cm² of surface area were employed; a simple calculation shows that such a cell should stop operating almost immediately if its capacity was limited by a several-nanometers-thick Li₂S layer. Finally, it is quite instructive to make a similar calculation for a conventional high surface area carbon. Let us assume the following electrode configuration: a 5 mg cm⁻² sulfur loading, a 1:1 ratio between carbon and the active sulfur on the carbon electrode, a carbon surface area of 500 m² g⁻¹, a uniform dense deposition, and a full discharge. In such an electrode the “passive film” would only be 1.7 nm thick, i.e., much below the usual threshold limit expected for completely insulating, defect-free materials (5–10 nm).²³ This strongly suggests that even if the deposition proceeded according to the 2D film-formation scenario, passivation cannot be the main reason for capacity limitation.

Here we show, using a variety of approaches, that even rather thick and seemingly compact discharge deposits do not, in fact, block the main polysulfide reactions and that the reasons for termination of battery operation are of a different nature, as discussed in detail in the last part of this paper. Interestingly, the same phenomenon is also identified in another advanced battery system: the magnesium–sulfur cell.

In order to discriminate between different scenarios, we use purposely designed electrochemical cells. Electrochemical techniques such as coulometric titration (galvanostatic method), impedance spectroscopy at open circuit voltage (OCV) or under bias, galvanostatic intermittent titration technique (GITT), and AC voltammetry are combined with complementary techniques for microstructural analysis, in particular focused ion beam–scanning electron microscopy (FIB-SEM) imaging and X-ray diffraction analysis.

2. EXPERIMENTAL SECTION

2.1. Materials and Cell Setup for the Li–S Battery System.

Experiments were conducted on cells assembled out of a 2 cm² glassy carbon (GC, HTW Germany) positive electrode (cathode) and a Li metal foil (110 μm, FMC) as the anode. Active species were added as catholyte solutions of various lithium polysulfide species dissolved in the supporting electrolyte consisting of 1 M LiTFSI in 1:1 (v:v) TEGDME:DOL. The separator type and thickness varied; either Celgard 2400 (25 μm) or GF/A glassy fiber separator (Whatman, 260 μm) were used, as specified in the individual case. The catholyte amount added to the pouch cell was dependent upon the thickness and number of separators used and is indicated with each measurement.

Porous electrodes were produced as 2 cm² discs by a doctor Blade application of the desired slurry. The ENSACO 350G carbon (Imerys) and a corresponding sulfur composite (ENSACO 350G/S) were prepared in a C:S = 1:2 mass ratio by melt infiltration under Ar atmosphere at 155 °C. The composite was mixed with a Printex (Degussa) conductivity additive and a PVdF binder in a mass ratio of 8:1:1 in NMP. Sulfur loading was approximately 1 mg/cm². Electrodes without sulfur were prepared using a similar procedure, by replacing the composite with as received ENSACO 350G carbon. The porous electrode surface area was on the order of 1000 cm²/cm² of the areal electrode surface. In some cases, carbon felt H14 (Freudenberg) was used as the positive electrode material. Its surface area was estimated to be 15 cm² per 1 cm² of geometric surface area.

All electrolyte solutions were prepared inside an Ar filled glovebox from previously dried solvents, salt, and polysulfide powder. The LiTFSI salt (Sigma-Aldrich, 99.95%) was dried overnight at 140 °C under vacuum, while solvents were dried in a multistep process using Al₂O₃, molecular sieves, and distillation, after which the water content was measured by Karl Fischer titration (Mettler Toledo, C20) and kept below 2 ppm. LiTDI salt (Solvionic, 99.9%) was used as received. The polysulfides were synthesized inside the glovebox by mixing the desired stoichiometric amounts of sulfur and metallic Li in THF at elevated temperature for a few days. After the solid precursor materials had reacted, the compounds were isolated inside the glovebox under reduced pressure. Since lithium polysulfides have a tendency to disproportionate in the used supporting electrolyte, the given concentrations of catholyte solutions should be considered nominal.

Pouch cells were assembled with electrodes with 2 cm² in geometric surface area. The exact amount of electrolyte or catholyte solution was added with a micropipette to the separator, after which the cell was stacked and vacuum sealed inside triplex foil (PET-Al-PE) with Ni contacts. The employed vacuum setting was tested to be such to ensure minimal loss of the electrolyte solvent.

2.2. Materials and Cell Setup for the Mg–S Battery System.

Magnesium polysulfides were synthesized as Mg[N-MeIm]₆S₈ complexes according to the procedure in ref 25. Catholyte solutions were prepared as 0.01 M Mg[N-MeIm]₆S₈ in 0.4 M MgTFSI₂ and 0.4 M MgCl₂ in 1:1 (v:v) TEGDME:DOL electrolyte. Before catholyte preparation, MgCl₂ (ultradry, Alfa Aesar, 99.99% metal trace) was used as it is and MgTFSI₂ (from Solvionic, 99.5%) was dried at 225 °C for 3 days.

Cathodes used in Mg–S experiments were the same as in the Li–S experiments. For the porous Mg–S cell discharge starting with sulfur, GF-A separator, 50 μL/mg of sulfur of the 0.4 M MgTFSI₂ and 0.4 M MgCl₂ in 1:1 (v:v) TEGDME:DOL electrolyte, and Mg metal foil (from Rich metals, 99.99%) were used. For the comparison of passivated porous electrode and pristine porous electrode without sulfur, GF-A separator, 50 μL of the above-mentioned catholyte solution, and Mg metal powder (prepared in the lab) were used. For the impedance tests with glassy carbon electrodes, GF-A separator, 50 μL of the above-mentioned catholyte solution, and Mg metal foil (from Rich metals, 99.99%) were used. In all cases, where Mg metal foil was used, it was brushed inside the glovebox prior to cell assembly to ensure activation of the anode.

2.3. Impedance Spectroscopy Measurements and Spectra Processing.

Electrochemical measurements were carried out using a Biologic VMP3 galvanostat/potentiostat. The spectra at open circuit voltage (OCV) conditions were measured with a voltage amplitude of 10 mV (rms). The measurements at different depths of discharge (DOD) were carried out after the cells had been discharged galvanostatically for a preselected amount of time. Prior to impedance measurements, the cells were relaxed at OCV conditions for 15 to 30 min, depending on the current magnitude employed previously. The voltage amplitude of the excitation signal was 10 mV (rms). Dynamic impedance measurements were done by superimposing the discharge current with a sinusoidal current signal with an amplitude of 10 to 20 times smaller than the discharge current itself. The frequency range varied according to the investigated phenomenon and was extended down to 20 μHz. As indicated in some cases, the number of measuring points was decreased in order to speed up the measurement.

2.4. SEM Imaging. For scanning electron microscopy analysis of the materials, a field-emission scanning electron microscope (FE SEM) Supra 35VP from Zeiss, Germany, and focused ion beam–scanning electron microscope (FIB-SEM) Helios Nanolab 650i (FEI, U.S.A.) were used. If the samples analyzed were sensitive to the atmosphere, they were prepared inside the glovebox on a custom-made holder, which was vacuumed inside the glovebox antechamber and opened when exposed to vacuum inside the SEM instrument. Discharged electrodes were briefly washed with THF prior to imaging in order to remove excess Li salt and long chain polysulfide species. Micrographs were usually collected with the electron gun accelerating

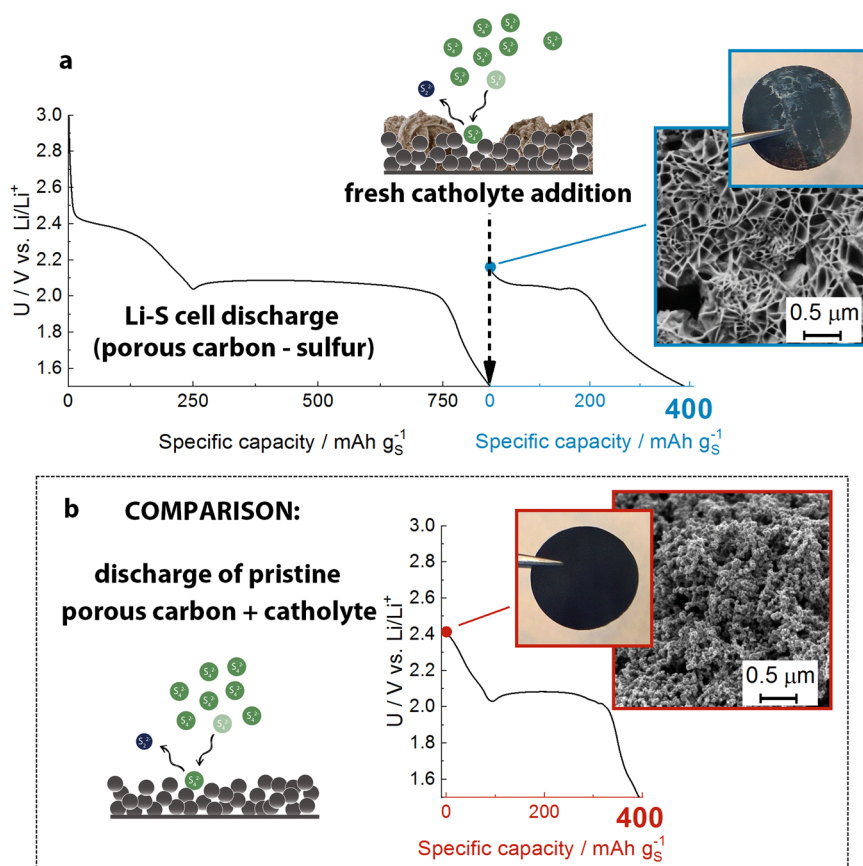


Figure 1. (a) Regular discharge of a conventional Li–S cell. After reaching a cut-off voltage of 1.5 V vs Li, the cell was disassembled and a fresh 0.1 M Li_2S_8 catholyte solution added according to the procedure described in Note 1 of the Supporting Information. The presumably passivated cathode delivered a capacity of about 400 mA h g^{-1} , a value comparable to a cell constructed from pristine porous carbon and the same catholyte (see panel b). The micrographs in panels (a) and (b) show the appearance of respective electrodes at blue and red points.

voltage of 1 kV, a low setting due to instability of the materials under the electron beam.

Samples intended for FIB cross-sectional analysis were attached on an Al-stub using a conductive carbon tape, vacuum sealed in a pouch bag inside the Ar filled glovebox, and transferred directly to the FIB instrument—without being exposed to air atmosphere at any point of the procedure. Sample cross sections were analyzed using FIB-SEM Helios Nanolab 650i (FEI, U.S.A.), equipped with a Pt gas injection system and energy dispersive spectrometer X-MAX 50 (Oxford, UK). Due to high sample sensitivity to the ion beam, the surface was initially protected with a 200 nm “in situ” deposited Pt film—induced with electron beam (2 kV @ 0.8 nA). Additional platinum was “in situ” deposited on top of the initial layer using a Ga^+ ion beam (30 kV @ 0.23 nA) to achieve a Pt surface protective layer with a final thickness of 800 nm. Cross sections were made using focused Ga^+ ions at 30 kV @ 2.5 nA with sequentially reducing currents down to 80 pA for the case of the final ion polishing step. Morphological images of the surface and cross sections were acquired using a low electron energy beam (2 kV @ 50 pA) and a standard ETD detector. Detailed information and phase contrast images on cross sections were acquired using InColumn integrated SE/BSE detectors and a premonochromated electron beam at 1 kV energy and 25 pA beam current.

3. RESULTS AND DISCUSSION

The discharge mechanism of the Li–S battery has been researched in significant detail. On the cathode (positive electrode) side the initial elemental sulfur is gradually reduced to soluble polysulfides of progressively smaller chain lengths. In the second part of a typical discharge curve Li_2S is formed

which, unlike the higher polysulfides, has a low solubility (reported values vary between $1.36 \times 10^{-3} \text{ M}$ and less than 10^{-20} M)^{18,26} and starts to intensely deposit on the surface of the underlying conductive electrode surface (usually a high-surface carbon). Li_2S itself is a very poor conductor with a conductivity on the order of $10^{-17} \text{ S cm}^{-1}$.^{7,27} It is therefore reasonable to expect that a thick and compact enough Li_2S deposit would block both the electronic and the ionic access to the underlying conductive carbon electrode. This should eventually lead to termination of battery operation. Indeed, many results in the literature indicate that such a scenario is very likely.^{4,8–15}

However, already a relatively simple experiment opens up many questions about the actual role of Li_2S in the Li–S battery operating mechanism. For example, Figure 1a shows a regular discharge of a freshly prepared conventional Li–S cell consisting of lithium as the anode and elemental sulfur as the cathodic material embedded in a porous high-surface area carbon (hereafter termed ENSACO/S composite). However, after reaching the usual lower cutoff limit (1.5 V vs Li, see arrow in Figure 1a) we did not proceed with charging—as usually done in battery research. Rather, we opened up the apparently fully discharged cell, washed the positive electrode to remove any soluble polysulfide species, and replaced the electrolyte with 20 μL of a 0.1 M Li_2S_8 catholyte solution in the conventional supporting electrolyte (for details see Note 1 of the Supporting Information). After carefully reassembling the cell, we continued the discharge of the cell instead of

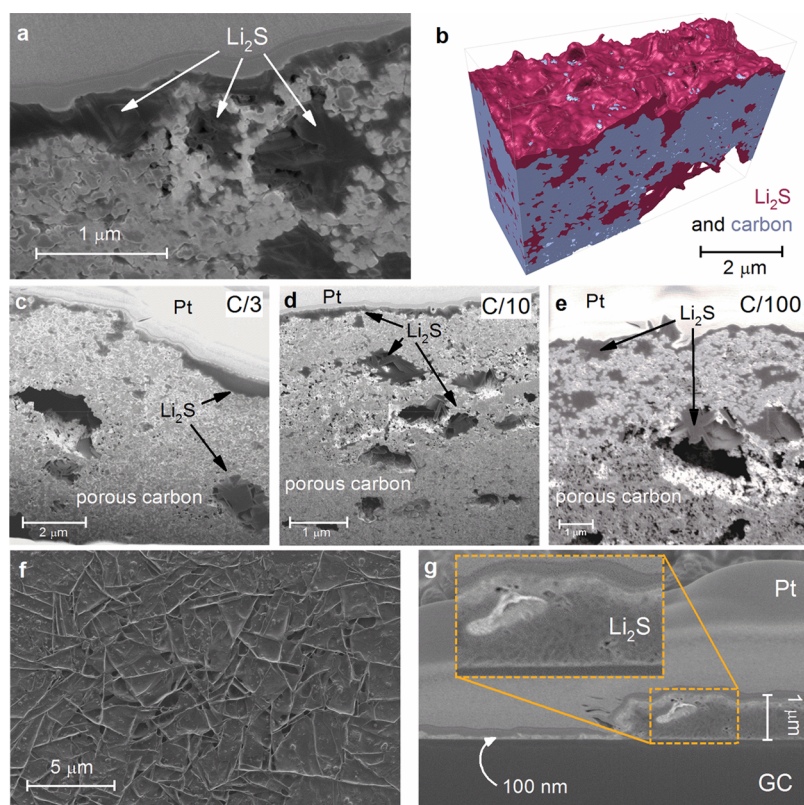


Figure 2. (a) SEM image of a cross section of the porous cathode discharged with C/10 current where the complex porous structure of Li_2S (dark gray) in the carbon matrix (light gray) is visible. (b) 3D tomography image of the top 3 μm section of the cathode discharged at C/100 with both carbon (light blue) and Li_2S (purple). Top surface of the box is equivalent to the actual top surface of the electrode (surface facing the separator). Blue areas on the top surface indicate parts of the carbon electrode not covered with the deposit. (c–e) cross sections of porous carbon electrodes discharged at a C/3, C/10, and C/100 current rates, respectively. (f, g) top view and cross-section SEM image of the Li_2S deposit on glassy carbon. A thick, porous structured deposit with the thickness in the range from below 100 nm up to $\sim 1 \mu\text{m}$ can be observed.

recharging it. The result is shown in Figure 1a, on the right of the dashed arrow. Obviously, almost half of the capacity delivered during the first regular discharge (Figure 1a) could still be achieved. This is in sharp contradiction with the widespread assumption that at the end of discharge the cathode is passivated due to the presence of a thick Li_2S or similar solid deposits,¹ the general appearance of which is demonstrated in the micrograph of Figure 1a. Comparing the capacities on the right and left sides of the dashed arrow in Figure 1a, one might argue that even if the solids do not completely passivate the surface at the end of regular discharge, they at least considerably limit the accessible surface area and, hence, a decrease in the capacity from ca. 800 mA h g^{-1} to ca. 400 mA h g^{-1} . However, note that in the first experiment elemental sulfur was used whereas in the second a solution of Li_2S_8 with lower theoretical capacity and a different level of accessibility to the porous carbon surface was utilized. Thus, a third experiment was carried out in which a pristine porous carbon in combination with a solution of Li_2S_8 was used (Figure 1b). The capacities of both setups containing Li_2S_8 are practically the same, although in one case the porous carbon cathode was considered completely passivated and in the other completely free of Li_2S deposit (pristine). Admittedly, however, the shapes of discharge curves do show some important differences. These are attributed to the different surface properties of carbon in both setups on the initial nucleation and growth of Li_2S crystallites, as discussed later on.

In an attempt to explain the intriguing results of Figure 1 we devised an additional series of experiments using different approaches and techniques. First, we investigated the properties of the solid discharge deposit in significant detail (Figure 2). SEM imaging in combination with 3D tomography imaging of various porous cathode slices (Figure 2a and Figure S1) reveal that large quantities of deposit exist both on the cathode surface and inside its pores. The general deposit's morphology is highly irregular and porous. To get a better understanding of the deposit distribution across the porous carbon matrix, sequential cross sections were obtained by cutting increasingly further into the electrode discharged at C/100 according to the procedure described in Note 2 of the Supporting Information. Using the obtained images, a 3D reconstruction was performed, yielding the tomography image of the Li_2S deposit as shown in Figure 2b (see additional images in Figure S2). The 3D images reveal several small areas on the outer surface of the electrode where Li_2S does not cover the carbon completely and the electrochemical reaction involving the remaining longer chained polysulfides can still take place. Further topological details about the deposit can be seen in two movies added to the Supporting Information. The observed thicker Li_2S deposits ($> 1 \mu\text{m}$) also explain the issues of the dissolution bottleneck revealed by other researchers when attempting to charge a Li–S battery cell.²⁸ Similarly, this finding helps us understand much better the reasons leading to the collapse of carbon matrix observed in some studies.^{29,30}

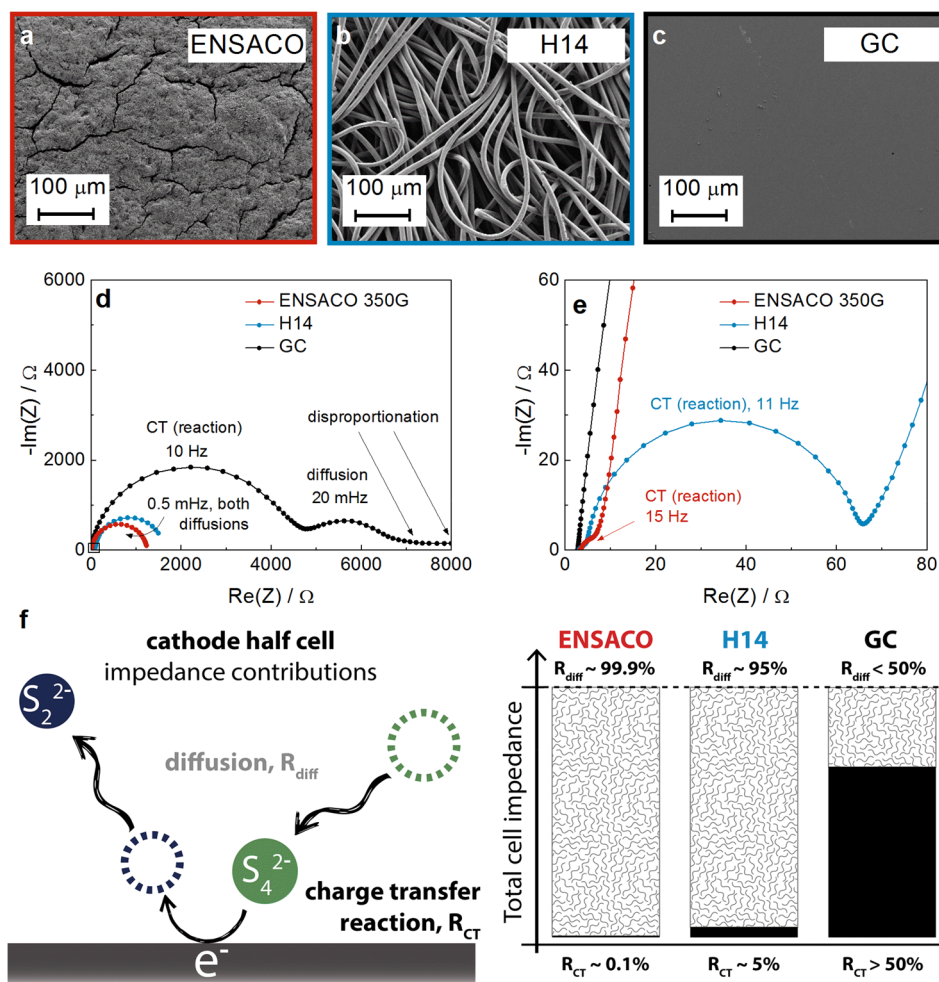


Figure 3. SEM images of the three types of carbon electrodes used: (a) ENSACO 350G porous electrode (total surface area, S_A , was 1000 cm² per 1 cm² of geometrical surface area), (b) H14 carbon felt ($S_A = 15$ cm²), and (c) glassy carbon electrode ($S_A = 1$ cm²). (d) Corresponding measured impedance spectra of three different symmetrical cells based on the three different types of carbon electrodes. (e) Magnification of the high-frequency region and the charge transfer contributions of both higher surface area electrodes. (f) Schematics showing the meaning of the main observed impedance features and their contributions to the total cell impedance, $Z_{\text{total}}(\text{OCV})$ (see comment in Note 4 of the Supporting Information).

Although the results presented so far indicate that the solid deposit detected in this study mainly corresponds to the final discharge product (Li_2S), one might argue that part of these deposits is due to unreacted sulfur which may remain in the system due to poor contact to the walls of porous carbon etc. In order to check this possibility, we carried out ex situ XRD analysis of a porous Li–S cathode measured after a C/10 discharge. The XRD pattern (Figure S3) revealed that during discharge all the α -sulfur peaks completely disappeared and three distinct diffraction peaks from Li_2S (denoted with arrows) appeared in the measured range. By considering peak broadening the mean crystallite size is found to be about 10 nm. This suggests that the observed large crystalline deposits (e.g., Figure 2a) are likely multidomain formations of Li_2S whereas the amount of unreacted sulfur, if present, is probably very small. These results are consistent with previous observations using *operando* XRD^{31,32} and *operando* XANES^{33,34} as discussed in Note 2 of the Supporting Information. Of course, these results do not preclude the possibility of significant sulfur remainders in other types of Li–S laboratory cells or in practical Li–S batteries.

Importantly, contrary to the literature reports¹⁶ we find that the main morphological features of the present deposit are largely independent of the C-rate used (Figure 2c–e, Figure S4). These results are inconsistent with the prevailing theory assuming that the main film growth mechanism is electro-deposition. If that was the case, the crystallite size should markedly depend on the C-rate. These inconsistencies call for a radical revision of the existing growth mechanism of solid deposit in Li–S cells during discharge, as proposed in the second part of this article.

As a whole, imaging techniques indicate that the solid deposit formed during discharge is highly porous and does not cover all of the available carbon surface. This might reasonably explain why it does not represent a significant barrier for penetration of electrolyte/catholyte into the inner parts of the cathode, thus allowing further discharge as demonstrated in Figure 1a.

However, one might argue that studying the deposit morphology under the conditions existing in a highly porous electrode cannot reveal all the essential features, such as typical deposit thickness, the degree of surface coverage, etc. Thus, we repeated the experiments by replacing the porous carbon

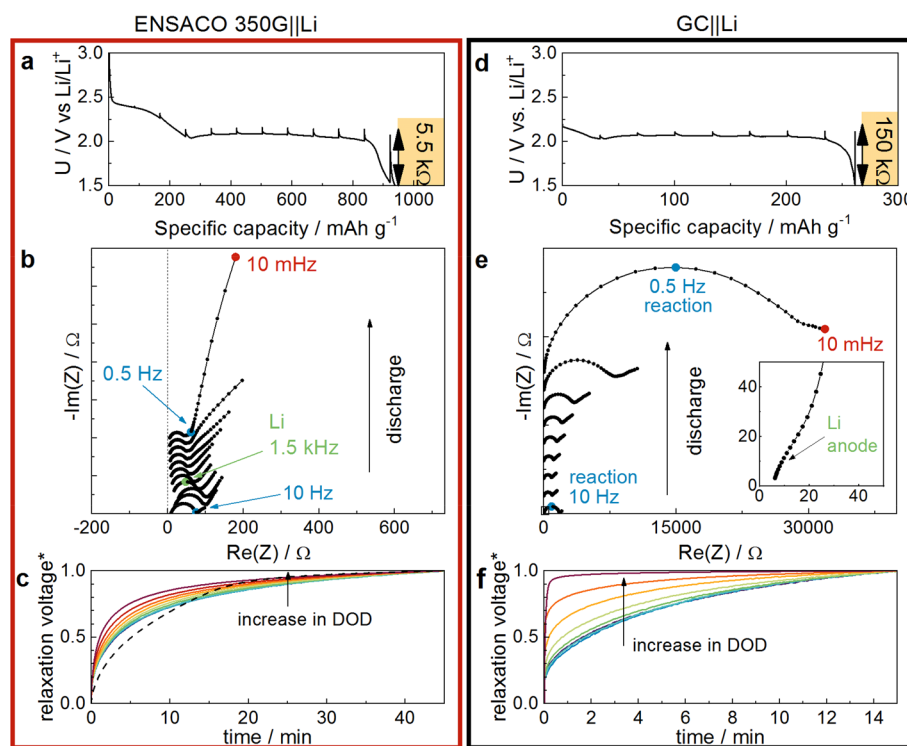


Figure 4. (a, d) Discharge voltage profiles with included relaxations (voltage increase) indicating the DOD where impedance was measured (at OCV) and the calculated value of the total cell resistance at the end of discharge for porous and flat surface electrode. (b, e) Impedance spectra at different DODs. Inset shows a magnification of the high frequency region of the first recorded spectrum, where the Li anode contribution is evident. (c, f) GITT measurement during discharge at the low voltage plateau of ENSACO||Li (during first 45 min) and GC||Li cell (15 min), respectively. *The absolute values of the voltages are normalized (see Supporting Information, Figure S7, for further elaboration).

cathode with a flat glassy carbon disc in conjunction with the same catholyte as used in Figure 1b. This way we considerably reduced the active surface area (from ca. 1000 cm² to 1 cm²) and amplified the probability of a “blocking nature” of the solid film; namely, in this case all the solid products are forced to deposit on the very limited flat surface area rather than spread into the interior of porous carbon.

The thickness and other morphological features of the deposit grown on flat glassy carbon were determined by a cross-section analysis using a focused ion beam–scanning electron microscope (FIB–SEM). Unexpectedly, the deposit was again found to be distinctively nonuniform, with thicknesses ranging from ~20 nm up to 1 μm (Figure 2fg and Figure S5). Namely, such a huge variation in thickness is incompatible with the widely accepted 2D layer mechanism of Li₂S film formation.^{16,17,20,21,35} This mechanism predicts that the film growth is uniform across the surface which means it should stop growing once a thickness of about several nanometers is reached (an upper value for electron tunnelling²³). It is thus very difficult to explain how such a very thick film, i.e., up to 50 times thicker than predicted, can grow based on the 2D layer mechanism. Even more surprisingly, despite this very big thickness we found that the deposit did not block the electrochemical reaction.

Whereas the experiments in Figure 1 rather directly point at a nonpassivating nature of the solid deposit on carbon, the more precise role of such a deposit in the overall electrochemical reaction/transport mechanism remains unclear. Furthermore, a more essential question emerges: if the cell operation is not limited by the solid deposited, what is then the main reason for the steep voltage decline in the last stage of

discharge curve? And, finally, if the size and morphology of the deposit are independent of the current rate used, what is the mechanism of Li₂S deposition? In order to find answers to these questions, we performed several dedicated experiments using different cell designs and electrochemical methods.

The main contributions to the total internal resistance of a typical Li–S cell at open circuit conditions were identified by simplifying the conventional Li–S cell configuration in different ways—while still retaining all the essential features related to cathode (electro)chemistry (see Note 3 of the Supporting Information). Impedance spectra of cathodes with different surface areas and degrees of porosity (Figure 3a,b) reveal two distinct features: a high-frequency arc due to charge transfer resistance (R_{CT}) and a low-frequency arc due to diffusion of polysulfides to the reaction sites on the carbon surface.^{24,36} As expected, the resistance of the polysulfide redox reaction (R_{CT}) decreases inversely proportionally to the available electrode surface area. Thus, in the case of highly porous ENSACO 350G carbon the R_{CT} contribution is practically negligible in comparison to the contribution of diffusion (resistance of diffusional arc > 1000 Ω, with a peak frequency around 0.5 mHz). In other words, the total impedance of cells based on porous carbon electrodes at open circuit conditions, $Z_{total}(OCV)$, is almost exclusively determined by diffusional processes whereas the reaction (charge transfer) part represents only a (very) small fraction of total impedance (much less than 1% in the high-surface area cathode configuration). It is important to note that this observation refers to a cathode in a partially discharged state, before any solid Li₂S deposit has formed.

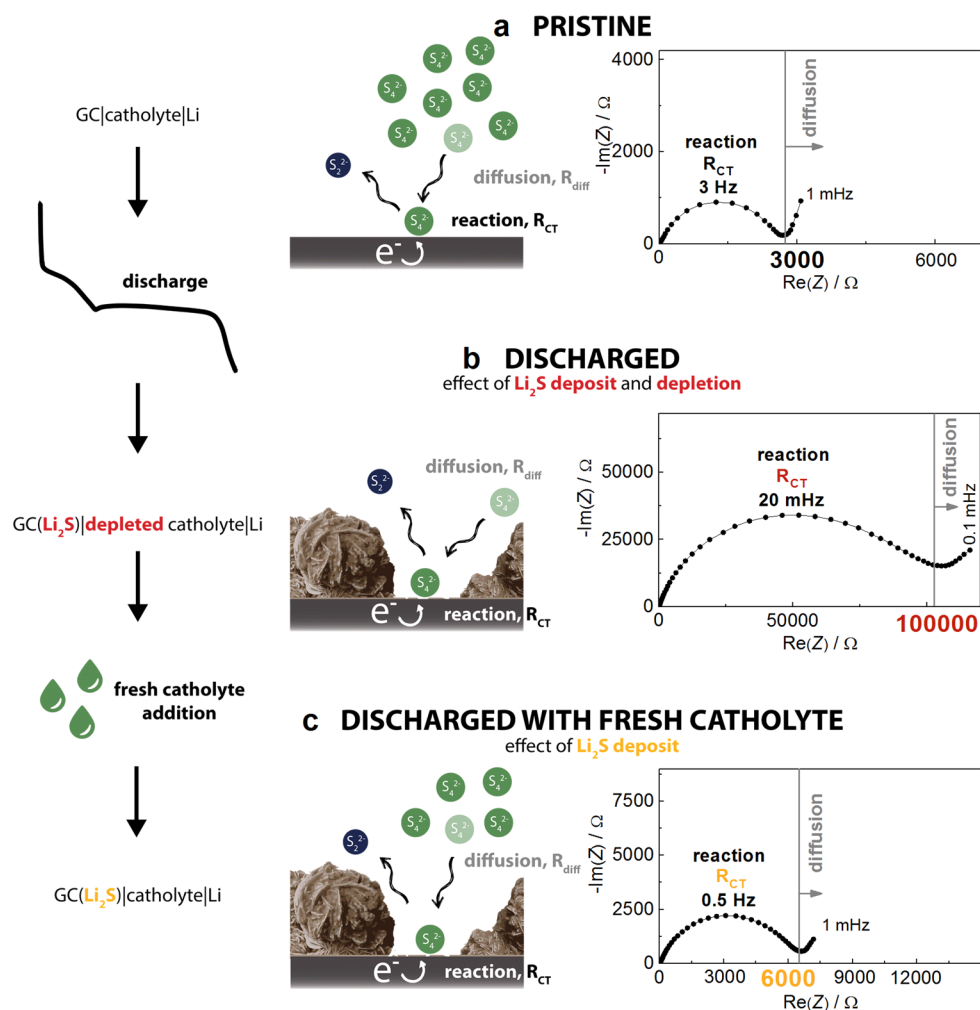


Figure 5. Schematic representation of the conducted experiment with shown conditions at the surface of the GC electrode and the corresponding measured impedance spectrum of (a) a pristine GC|catholyte|Li cell; (b) a GC(Li₂S)||Li cell after prolonged discharge with Li₂S deposit and depleted electrolyte; and (c) the same discharged GC(Li₂S)||Li cell with a Li₂S deposit, where fresh catholyte was added.

Based on this observation one can hypothesize as follows: even if during the following discharge a very large portion (e.g., 95%) of a conventional porous carbon electrode surface is covered with an insulating layer (reducing the available electrode area by a factor of 20), the charge transfer contribution will still be much smaller than that of the diffusional impedance. In other words, it seems that in conventional cells with high surface area (porous) carbon electrodes the cell operation will be controlled by polysulfide diffusion (mass transfer) rather than by polysulfide electrochemical reaction. This hypothesis is consistent with the proposed scenario in a recent rate-capability study.³⁷

So far, the electrode dynamics were studied on pristine carbons—in the absence of any surface deposits. For the present purpose, however, it was essential to monitor the development of transport-reaction contributions during the discharge, especially in the region where deposition of solid film is expected. Three central experiments along this line are shown in Figure 4 (see Note 5 of the Supporting Information for experiment design). For easier comparison, “total cell resistances” were calculated from overvoltages determined from the relaxation part of the experiment (Figure 4a,d, see also Note 6 of the Supporting Information). One can see that both the total cell resistance (Figure 4a,d) and the absolute

value of impedance at lowest frequencies (Figure 4b,e) consistently increase toward the end of discharge. Also, it is evident that the values of both parameters increase as we decrease the surface area of the cathode. However, already a rough comparison between the galvanostatic and impedance measurements shows a large mismatch in observed resistances, for example, 150 kΩ:30 kΩ and 5.5 kΩ:0.5 kΩ for the glassy carbon and ENSACO electrode, respectively. Most importantly, we can see that in both cases the value of reaction resistance is much smaller, at least by a factor of 5, than the total cell resistance.

Clearly, impedance spectroscopy measurements at the open circuit condition cannot be used to directly probe the rate-limiting process at the very end of discharge because the system tends to undergo very fast voltage drift (rise) during relaxation in the direction of quasi-equilibrium. In order to understand the underlying causes for the final voltage drop, GITT relaxation curves were examined (Figure 4c,f). For the cell based on the glassy carbon electrode (Figure 4f) it is evident that, with an increase in DOD, fast processes start to dominate the overpotential (purple curve in Figure 4f shows >90% of relaxation in voltage in the first 60 s of the experiment). The latter result can be directly compared with the impedance response (Figure 4e) where the reaction arc

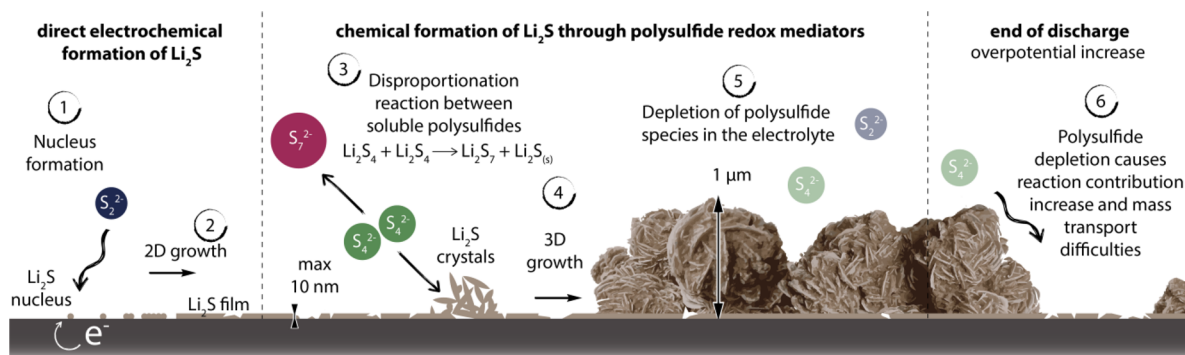


Figure 6. Scheme of the proposed Li_2S deposition mechanism through the initial electrochemical, followed by predominantly chemical formation of Li_2S . During continuous cell operation both mechanisms can take place in parallel. Regardless of the mechanism, the formation of a thick deposit inevitably leads to significant depletion of polysulfide species in the electrolyte.

with a typical time constant of ~ 2 s ends at about (40–10) mHz—corresponding to a typical relaxation time of ~ 25 –100 s.

This observation demonstrates that in the case of severe limitations in the cathode surface area (planar electrode) the end of discharge is dominated by the reactional resistance. By contrast, all the GITT relaxation curves for porous carbon cathode (Figure 4c) suggest that slow process(es) (time scale $\gg 1$ min) are limiting the cell performance whereas the IR drop together with the reaction resistance remains similar in all curves measured (see also Figure S7). We argue that only the bulk transport (polysulfide diffusion) can be a cause of such a slow relaxation. While already being slow due to the inherently low diffusion coefficient of polysulfides, this transport may be further impeded in cases when either the electrode and/or the deposits exhibit significant tortuosity. At least in principle, the effect of the latter can elegantly be checked using impedance spectroscopy as demonstrated recently,³⁸ which will probably be a topic of our forthcoming studies.

The crucial role of slow diffusion of polysulfides in cell performance limitation is supposed to be valid quite generally, regardless of the exact composition of the deposit (note that it may contain various solid products including some unreacted sulfur etc.)—as long as this deposit exhibits some porosity and the diffusion length is on the order of micrometers or longer. To summarize, although also in the case of conventional porous carbon electrodes the reaction resistance does increase toward the end of cell discharge, the resistance due to diffusion of polysulfides is consistently much higher and represents a clear rate-limiting step along the whole discharge curve.

In order to further check the validity of this essential finding, we employed two additional “dynamic” techniques that probed the system under operation conditions: (1) the so-called dynamic impedance measurements (Figure S8) and (2) alternating current voltammetry (ACV, Figure S9). Both additionally confirmed the findings gathered from experiments in Figure 4.

Now, if diffusion of polysulfides toward the active porous carbon cathode is the rate-limiting process during the whole discharge, it is reasonable to speculate that the final rapid overvoltage increase (potential drop) is also due to progressively decreasing diffusional flux of active species toward the active electrochemical centers for polysulfide reaction. This suggests that, most likely, the essential problem during the last stage(s) of discharge is simply a relatively rapid decrease of concentration of polysulfides at the electrode

(active) surface. This assumption could be relatively easily checked—by employing a similar strategy as used during the initial experiments shown in Figure 1—however using a more defined system and additional methods such as impedance spectroscopy.

Thus, we used a flat rather than porous electrode—for better control of formation of solid deposit. Before forming as thick as possible a deposit according to a procedure similar to the one shown previously (see Figure 2f,g and Figure S10), we measured the impedance response of the pristine cell (Figure 5a). Impedance measurements were also used at the end of the procedure of thick deposit formation (Figure 5b). Then the cell was opened inside an Ar-filled glovebox and a fresh catholyte solution was added. A large reduction of the reaction arc was observed (compare Figure 5b and Figure 5c showing a 16-fold decrease of arc). In fact the size of the impedance arc immediately dropped relatively close to the initial value of about $3 \text{ k}\Omega$ found for a completely pristine electrode without any Li_2S deposit (Figure 5a). This strongly suggests that the effect of Li_2S deposition on reaction impedance is much smaller than the effect of catholyte (polysulfide) concentration decrease, as schematically shown in Figure 5. This hypothesis is further supported by a comparison of impedance spectra measured under potential bias and the corresponding quasi-steady-state current responses (Figures S11–S13).

Finally, based on the results of experiments carried out in this work, we may propose a new mechanism of deposit formation which is able to consistently explain all the observed phenomena while also reconciling the apparently contradictory observations in the literature. As mentioned, the observed morphological features of deposits and their independence of the C-rate, both on flat and porous electrodes, are in sharp contradiction with fundamental predictions of the widely accepted 2D model of deposit growth. Here we propose a more complex mechanism which also takes into account the chemically driven formation of deposit—besides the purely electrochemically driven growth as assumed in the 2D model. A central role in the chemically driven part of the mechanism is given to the known strong tendency of polysulfides toward disproportionation,^{15,24,39} through which longer-chained polysulfides act as redox mediators for Li_2S deposition (scheme, Figure 6). This means that a large portion of the Li_2S is formed chemically rather than electrochemically.

We propose that in the first step nucleation and probably some 2D growth takes place—as we consider this to be more energetically favorable compared to a direct chemical

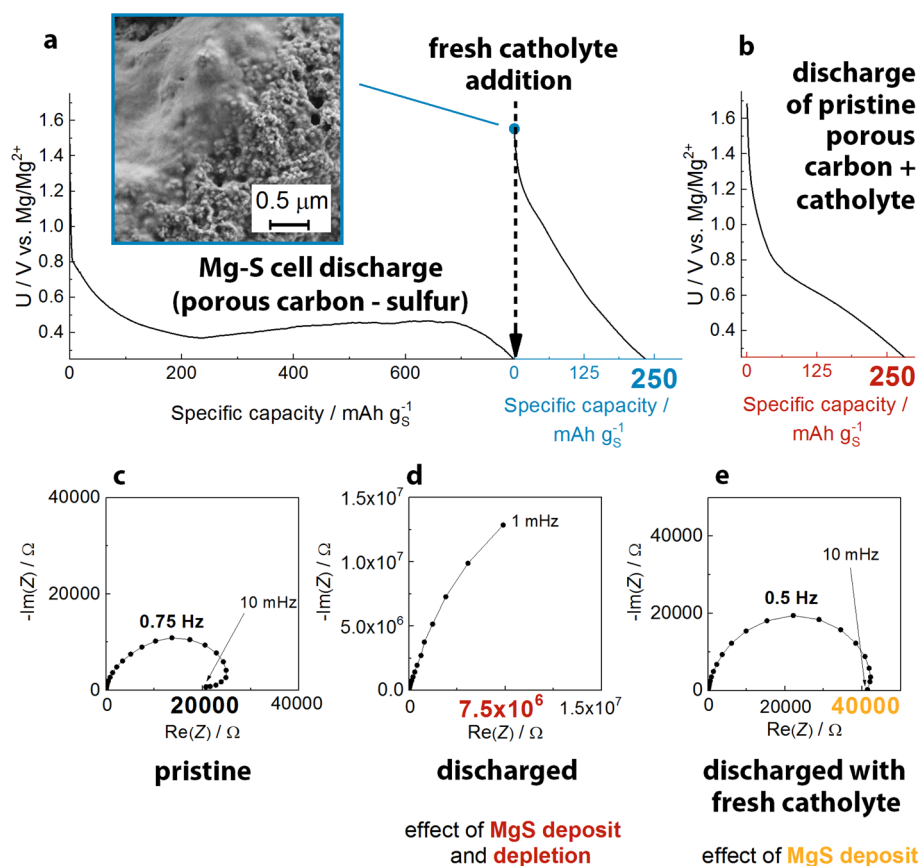


Figure 7. Experiments on typical magnesium–sulfur electrochemical cell showing results similar to those of the lithium–sulfur cells. (a) Regular discharge of a conventional Mg–S cell. After reaching a cut-off voltage of 0.25 V vs Mg, the cell was disassembled and fresh 0.01 M MgS_8 catholyte solution added. The presumably passivated cathode delivered a capacity of about 250 mA h g^{-1} , a value comparable to a cell constructed from pristine porous carbon and the same catholyte (see panel b). The micrograph in panels (a) show the appearance of the electrode at the blue point. (c) Impedance spectrum for the pristine GC|catholyte|Mg cell; (d) GC(MgS)||Mg cell after prolonged discharge with MgS deposit and depleted electrolyte; and (e) the same discharged GC(MgS)||Mg cell with MgS deposit, where fresh catholyte was added.

precipitation from solution. However, once nuclei/small 2D patches of Li_2S have formed on the carbon surface, these can serve as “anchors” for rather rapid and extensive 3D deposition of Li_2S driven by disproportionation reactions. Later on, both mechanisms can take place simultaneously yielding a morphologically complex deposit as indeed detected by direct observation. We note that additional morphological complication might arise if—due to poor electric contacting etc.—some of the initial sulfur remains unreacted throughout the discharge (though in the present specific experiments such unreacted sulfur was not detected).

As the 2D growth mechanism can only take place at the three-phase boundary of the already formed deposit whereas the chemically driven 3D growth proceeds on any chosen surface of solid Li_2S deposits, we assume the latter growth mode to prevail. In particular, this reasoning can easily explain the observed wide-range variation of deposit thickness (from several nanometers up to a micrometer). In fact, this wide range alone demonstrates the extreme level of deposit nonuniformity, especially when having in mind that a uniform, defect-free film extending over the whole surface area would only be 1.7 nm thick, as can easily be calculated from known compositional and geometrical parameters of porous carbon electrode cells used in this work. In terms of electrochemistry such morphological nonuniformity translates into very poorly expressed, if any, passivating properties.

The intensive chemical formation of the Li_2S -based deposit can also explain the rapid increase of overvoltage toward the end of discharge causing premature end of cell operation. Although the formed deposit itself does not significantly block the cathode surface reaction, its rapid formation depletes the surrounding electrolyte solution of electroactive species. In principle the consumption of polysulfides from the solution is expected as this is the main underlying concept of Li–S battery cell operation. However, this very concept anticipates that the concentration of polysulfides will gradually drop in the whole electrolyte volume until all the polysulfides have been consumed. By contrast, as the present experiments strongly suggest, the rapid formation of a large amount of solid deposits depletes the concentration predominantly at the electrode/electrolyte interface.

Finally, we were wondering whether this “non-passive” nature of large surface deposits was limited to the Li–S cell or could this phenomenon have a wider significance and would be found in other modern systems exploiting surface reactions such as Li–air, Mg–sulfur, etc. Based on our experience with the Mg–sulfur system, we decided to repeat the essential experiments shown above also on a typical Mg–sulfur cell (Figure 7).

Specifically, we tested whether the conventional porous electrode was passivated after the end of discharge also in the Mg–S cell (direct comparison with Figure 1) and how the

impedance changed after prolonged discharge and upon addition of fresh polysulfide species (to compare the behavior with Figure 5). As evident from Figure 7, the magnesium–sulfur cell shows very similar behavior as demonstrated for the lithium–sulfur cell. For example, the capacity obtained using the already “passivated” electrode is almost identical to the one obtained from the discharge of the pristine porous carbon cell with catholyte solution (compare Figure 7a with Figure 7b). Similarly as in the case of Li, the discharged electrode was examined under SEM (micrograph in blue squares) and showed a film-like deposit on the surface of the carbon particles. The absence of crystalline particles is in line with previous reports for discharged magnesium–sulfur electrodes.⁴⁰ Although in this case the deposit is probably amorphous rather than crystalline, it can reasonably be assumed that it precipitates in a similar solution-mediated fashion and, most importantly, does not electrochemically block the surface reactions. This is corroborated with the three-step impedance measurements (Figure 7c–e) using a flat glassy carbon substrate. Very similar as in the case of lithium, after prolonged discharge (C/200 and constant voltage hold at 0.25 V vs Mg for 24 h), the initial arc size of 20 k Ω (Figure 7d) increases by several orders of magnitude (to ca. 20 M Ω , Figure 7d). After the discharge, the cell was opened inside a glovebox and fresh magnesium polysulfide solution was added—without changing the separator or magnesium anode. Subsequently, the impedance of this cell greatly decreased, indicating that (i) the magnesium anode was not the source of the increase of impedance at the end of discharge and (ii) depletion of magnesium polysulfides is again the lead cause behind overpotential increase.

At a first glance the similar behaviors of Li–S and Mg–S—that is, two systems with significantly different chemistries—could be surprising. However, the surface film properties are largely determined by its growth mechanism and based on present results it is reasonable to assume that both proceed according to the general mechanism displayed in Figure 6. In other words, if the electrochemical deposition is strongly interfered with by rapid chemically driven deposition, one can expect the final deposit to be porous and full of defects, inclusions, and other irregularities, leading to very poor surface protection.

4. CONCLUSIONS

We showed—using several independent approaches, different electrode types, and innovative cell design—that the occurrence of solid deposits in a typical Li–S cell does not essentially block the main electrochemical reaction. Interestingly, the same phenomenon was observed for an essentially different system: magnesium–sulfur. Although the solid deposits are locally even thicker (up to 1 μm) than usually assumed, they are extremely nonuniform in thickness (the latter may vary from several nanometers to 1 μm) and considerably porous, both of which allows relatively unhindered penetration of active polysulfides across the deposit to the active carbon surface. The unusual morphological features of the deposit were explained by upgrading the prevalent 2D film formation mechanism with another step, that is, chemically driven deposition based on the well-known tendency of polysulfides to disproportionate. A natural consequence of the proposed mechanism is a (strong) depletion of polysulfide concentration in the surrounding electrolyte solution. Dedicated experiments confirmed that

indeed the faster-than-expected polysulfide depletion is probably the main culprit for (premature) termination of cell operation. The depleted polysulfides cannot be efficiently compensated for by those that are still present in more distant areas, such as within the relatively thick separator, as the diffusion of those “wandering” polysulfides toward the active surface of positive electrode proceeds very slowly. This slow diffusion generates high impedance values already over distances on the micrometer range, as demonstrated in our previous work.²⁴

An ultimate approach that would mitigate the complications due to polysulfide depletion would be to use an ion-selective interlayer between the cathode and the separator or other measures for effective retention of polysulfides inside the cathode composite. Another commonly met proposal for improvement of Li–S battery performance is through decreasing the electrolyte-to-sulfur ratio. However, at least in the case of the present electrolyte system, such a strategy may be questionable. First we note that combining a high sulfur loading with a low electrolyte/sulfur ratio (a setup intended for practical applications), polysulfide saturation is eventually reached. Generally, maximization of the concentration of active species is desirable as it tends to minimize the overpotentials due to diffusion and reaction which ultimately can increase the practical capacity. However, in some cases (and notably in the present system) the increase in concentration is accompanied by significant increase in viscosity of the electrolyte solution. If the latter prevails, the polysulfide transport can be negatively affected and the corresponding overpotential exceedingly increases before the start of the second plateau where Li₂S deposition begins. In extreme cases the cutoff voltage may be reached prematurely and the cell capacity severely reduced.

In any case, when designing improved Li–S cells by maximizing the sulfur content, one can keep the specific surface area of the cathode at moderate values. This results directly from the present finding that capacity is not limited with the blockage of the cathode surface with insoluble insulating deposit. Similarly, the study refutes the capacity fade mechanism through loss of contact between Li₂S particles and the electrode surface, since (chemical) redox reactions between sulfur species can still continue in solution. The present results strongly indicate that in the conventionally used electrolytes there is no need for expensive redox mediator additives, when added in the attempt of promoting 3D growth of the solid deposition product during discharge—since polysulfide species themselves act as such.

Finally, we argue that all of the findings presented in this work are also potentially relevant for improved understanding of other electrochemical systems involving soluble intermediates that can interact and disproportionate, in particular magnesium–sulfur as partly demonstrated in the last experiment and also Li–air batteries.

■ ASSOCIATED CONTENT

Supporting Information

The Supporting Information is available free of charge on the ACS Publications website at DOI: 10.1021/acs.chemmater.9b03255.

Note 1, experimental details on extending the discharge of battery cells by adding fresh catholyte and SEM imaging of various cathode surface and pores; note 2,

three-dimensional microstructural analysis parameters, XRD ex situ determination of the main components consisting the solid deposits in discharged Li–S cathode; investigation of Li₂S morphology obtained at different current rates; and cross-section analysis of a glassy carbon electrode with Li₂S deposit; Note 3, reasons for the study and implementation of model experiments with glassy carbon electrodes; note 4, comment on the total cell impedance, $Z_{total}(OCV)$, of symmetric cathode/cathode cells measured in quasi-equilibrium at open circuit conditions; note 5, cell and measurement setup for the study of EIS evolution during discharge; and note 6, total cell resistance (R_{total}) of a Li–S battery during electrochemical operation, GITT analysis, dynamic impedance spectroscopy measurement for the GC|catholyte|Li cell; alternating current voltammetry; experiments of prolonged Li₂S deposition; and impedance spectroscopy of GC||Li cells under bias in quasi-steady state (PDF)

Topological details of the Li₂S deposit (MOV)

Topological details of the Li₂S deposit (MOV)

AUTHOR INFORMATION

ORCID

Alen Vizintin: 0000-0003-1876-1396

Robert Dominko: 0000-0002-6673-4459

Miran Gaberšček: 0000-0002-8104-1693

Notes

The authors declare no competing financial interest.

ACKNOWLEDGMENTS

This work was financially supported by Slovenian Research Agency (ARRS, Programme No. P2-0393) and through Helix project (European Union's Horizon 2020 research and innovation program under Grant Agreement No. 666221). We also gratefully acknowledge the financial support from Honda R&D Europe (Germany).

REFERENCES

- (1) Su, Y.-S.; Manthiram, A. Lithium–Sulphur Batteries with a Microporous Carbon Paper as a Bifunctional Interlayer. *Nat. Commun.* **2012**, *3*, 1166.
- (2) Ji, X.; Lee, K. T.; Nazar, L. F. A Highly Ordered Nanostructured Carbon–Sulphur Cathode for Lithium–Sulphur Batteries. *Nat. Mater.* **2009**, *8*, 500–506.
- (3) Wang, L.; Wang, Y.; Xia, Y. A High Performance Lithium-Ion Sulfur Battery Based on a Li₂S Cathode Using a Dual-Phase Electrolyte. *Energy Environ. Sci.* **2015**, *8*, 1551–1558.
- (4) Demir-Cakan, R.; Morcrette, M.; Gangulibabu; Guéguen, A.; Dedryvère, R.; Tarascon, J.-M. Li–S Batteries: Simple Approaches for Superior Performance. *Energy Environ. Sci.* **2012**, *6*, 176–182.
- (5) Drvarič Talian, S.; Jeschke, S.; Vizintin, A.; Pirnat, K.; Arčon, I.; Aquilanti, G.; Johansson, P.; Dominko, R. Fluorinated Ether Based Electrolyte for High-Energy Lithium–Sulfur Batteries: Li⁺ Solvation Role Behind Reduced Polysulfide Solubility. *Chem. Mater.* **2017**, *29*, 10037–10044.
- (6) Cuisinier, M.; Cabelguen, P.-E.; Adams, B. D.; Garsuch, A.; Balasubramanian, M.; Nazar, L. F. Unique Behaviour of Nonsolvents for Polysulphides in Lithium–Sulphur Batteries. *Energy Environ. Sci.* **2014**, *7*, 2697–2705.
- (7) Kim, B. S. D.-H.; Lee, M. S. B.; Park, K.-Y.; Kang, K. First-Principles Study on the Charge Transport Mechanism of Lithium Sulfide (Li₂S) in Lithium-Sulfur Batteries. *Chem. - Asian J.* **2016**, *11*, 1288–1292.
- (8) Lang, S. Y.; Shi, Y.; Guo, Y. G.; Wang, D.; Wen, R.; Wan, L. J. Insight into the Interfacial Process and Mechanism in Lithium–Sulfur Batteries: An In Situ AFM Study. *Angew. Chem., Int. Ed.* **2016**, *55*, 15835–15839.
- (9) Liu, Z.; Mukherjee, P. P. Mesoscale Elucidation of Surface Passivation in the Li-Sulfur Battery Cathode. *ACS Appl. Mater. Interfaces* **2017**, *9*, S263–S271.
- (10) Barchasz, C.; Leprêtre, J. C.; Alloin, F.; Patoux, S. New Insights into the Limiting Parameters of the Li/S Rechargeable Cell. *J. Power Sources* **2012**, *199*, 322–330.
- (11) Canas, N. A.; Hirose, K.; Pascucci, B.; Wagner, N.; Friedrich, K. A.; Hiesgen, R. Investigations of Lithium-Sulfur Batteries Using Electrochemical Impedance Spectroscopy. *Electrochim. Acta* **2013**, *97*, 42–51.
- (12) Busche, M. R.; Adelhalm, P.; Sommer, H.; Schneider, H.; Leitner, K.; Janek, J. Systematical Electrochemical Study on the Parasitic Shuttle-Effect in Lithium-Sulfur-Cells at Different Temperatures and Different Rates. *J. Power Sources* **2014**, *259*, 289–299.
- (13) Noh, H.; Song, J.; Park, J.-K.; Kim, H.-T. A New Insight on Capacity Fading of Lithium–Sulfur Batteries: The Effect of Li₂S Phase Structure. *J. Power Sources* **2015**, *293*, 329–335.
- (14) Waluś, S.; Barchasz, C.; Bouchet, R.; Martin, J. F.; Leprêtre, J. C.; Alloin, F. Investigation of Non-Woven Carbon Paper as a Current Collector for Sulfur Positive Electrode—Understanding of the Mechanism and Potential Applications for Li/S Batteries. *Electrochim. Acta* **2016**, *211*, 697–703.
- (15) Xu, R.; Lu, J.; Amine, K. Progress in Mechanistic Understanding and Characterization Techniques of Li-S Batteries. *Adv. Energy Mater.* **2015**, *5*, 1500408.
- (16) Fan, F. Y.; Carter, W. C.; Chiang, Y.-M. Mechanism and Kinetics of Li₂S Precipitation in Lithium-Sulfur Batteries. *Adv. Mater.* **2015**, *27*, S203–S209.
- (17) Fan, F. Y.; Chiang, Y.-M. Electrodeposition Kinetics in Li-S Batteries: Effects of Low Electrolyte/Sulfur Ratios and Deposition Surface Composition. *J. Electrochem. Soc.* **2017**, *164*, A917–A922.
- (18) Thangavel, V.; Xue, K.-H.; Mameri, Y.; Quiroga, M.; Mastouri, A.; Guéry, C.; Johansson, P.; Morcrette, M.; Franco, A. A. Microstructurally Resolved Model for Li-S Batteries Assessing the Impact of the Cathode Design on the Discharge Performance. *J. Electrochem. Soc.* **2016**, *163*, A2817–A2829.
- (19) Peng, H. J.; Zhang, G.; Chen, X.; Zhang, Z. W.; Xu, W. T.; Huang, J. Q.; Zhang, Q. Enhanced Electrochemical Kinetics on Conductive Polar Mediators for Lithium–Sulfur Batteries. *Angew. Chem., Int. Ed.* **2016**, *55*, 12990–12995.
- (20) Gerber, L. C. H.; Frischmann, P. D.; Fan, F. Y.; Doris, S. E.; Qu, X.; Scheuermann, A. M.; Persson, K.; Chiang, Y.-M.; Helms, B. A. Three-Dimensional Growth of Li₂S in Lithium–Sulfur Batteries Promoted by a Redox Mediator. *Nano Lett.* **2016**, *16*, 549–554.
- (21) Kim, K. R.; Lee, K.-S.; Ahn, C.-Y.; Yu, S.-H.; Sung, Y.-E. Discharging a Li-S Battery with Ultra-High Sulphur Content Cathode Using a Redox Mediator. *Sci. Rep.* **2016**, *6*, 32433.
- (22) Pan, H.; Chen, J.; Cao, R.; Murugesan, V.; Rajput, N. N.; Han, K. S.; Persson, K.; Estevez, L.; Engelhard, M. H.; Zhang, J.-G.; et al. Non-Encapsulation Approach for High-Performance Li–S Batteries through Controlled Nucleation and Growth. *Nat. Energy* **2017**, *2*, 813–820.
- (23) Moffat, T. P.; Yang, H.; Fan, F.-R. F.; Bard, A. J. Electron-Transfer Reactions on Passive Chromium. *J. Electrochem. Soc.* **1992**, *139*, 3158–3167.
- (24) Drvarič Talian, S.; Moškon, J.; Dominko, R.; Gaberšček, M. Reactivity and Diffusivity of Li Polysulfides: A Fundamental Study Using Impedance Spectroscopy. *ACS Appl. Mater. Interfaces* **2017**, *9*, 29760–29770.
- (25) Bieker, G.; Wellmann, J.; Kolek, M.; Jalkanen, K.; Winter, M.; Bieker, P. Influence of Cations in Lithium and Magnesium Polysulphide Solutions: Dependence of the Solvent Chemistry. *Phys. Chem. Chem. Phys.* **2017**, *19*, 11152–11162.
- (26) Cheng, L.; Curtiss, L. A.; Assary, R. S.; Narayanan, B.; Redfern, P. Reaction Mechanisms in Li-S Batteries Determined by Solubilities

of Li Polysulfides. Presented at the LiSM3, Chicago, IL, USA, 25–26 April, 2018.

(27) Park, H.; Kumar, N.; Melander, M.; Vegge, T.; Garcia Lastra, J. M.; Siegel, D. J. Adiabatic and Nonadiabatic Charge Transport in Li-S Batteries. *Chem. Mater.* **2018**, *30*, 915–928.

(28) Marinescu, M.; O'Neill, L.; Zhang, T.; Walus, S.; Wilson, T. E.; Offer, G. J. Irreversible vs Reversible Capacity Fade of Lithium-Sulfur Batteries during Cycling: The Effects of Precipitation and Shuttle. *J. Electrochem. Soc.* **2018**, *165*, A6107–A6118.

(29) Barai, P.; Mistry, A.; Mukherjee, P. P. Poromechanical Effect in the Lithium–Sulfur Battery Cathode. *Extrem. Mech. Lett.* **2016**, *9*, 359–370.

(30) Elazari, R.; Salitra, G.; Talyosef, Y.; Grinblat, J.; Scordilis-Kelley, C.; Xiao, A.; Affinito, J.; Aurbach, D. Morphological and Structural Studies of Composite Sulfur Electrodes upon Cycling by HRTEM, AFM and Raman Spectroscopy. *J. Electrochem. Soc.* **2010**, *157*, A1131–A1138.

(31) Conder, J.; Bouchet, R.; Trabesinger, S.; Marino, C.; Gubler, L.; Villevieille, C. Direct Observation of Lithium Polysulfides in Lithium–Sulfur Batteries Using Operando X-Ray Diffraction. *Nat. Energy* **2017**, *2*, 17069.

(32) Schneider, A.; Weidmann, C.; Suchomski, C.; Sommer, H.; Janek, J.; Brezesinski, T. Ionic Liquid-Derived Nitrogen-Enriched Carbon/Sulfur Composite Cathodes with Hierarchical Microstructure—a Step toward Durable High-Energy and High-Performance Lithium-Sulfur Batteries. *Chem. Mater.* **2015**, *27*, 1674–1683.

(33) Dominko, R.; Patel, M. U. M.; Lapornik, V.; Vizintin, A.; Koželj, M.; Tušar, N. N.; Arčon, I.; Stievano, L.; Aquilanti, G. Analytical Detection of Polysulfides in the Presence of Adsorption Additives by Operando X-Ray Absorption Spectroscopy. *J. Phys. Chem. C* **2015**, *119*, 19001–19010.

(34) Kavčič, M.; Bučar, K.; Petric, M.; Žitnik, M.; Arčon, I.; Dominko, R.; Vizintin, A. Operando Resonant Inelastic X-Ray Scattering: An Appropriate Tool to Characterize Sulfur in Li–S Batteries. *J. Phys. Chem. C* **2016**, *120*, 24568–24576.

(35) Tian, B.; Ning, G.-H.; Tang, W.; Peng, C.; Yu, D.; Chen, Z.; Xiao, Y.; Su, C.; Loh, K. P. Polyquinoneimines for Lithium Storage: More than the Sum of Its Parts. *Mater. Horiz.* **2016**, *3*, 429–433.

(36) Adamič, M.; Drvarič Talian, S.; Sinigoj, A. R.; Humar, I.; Moškon, J.; Gaberšček, M. A Transmission Line Model of Electrochemical Cell's Impedance: Case Study on a Li-S System. *J. Electrochem. Soc.* **2019**, *166*, A5045–A5053.

(37) Zhang, T.; Marinescu, M.; Walus, S.; Kovacic, P.; Offer, G. J. What Limits the Rate Capability of Li-S Batteries during Discharge: Charge Transfer or Mass Transfer? *J. Electrochem. Soc.* **2018**, *165*, A6001–A6004.

(38) Raccichini, R.; Furness, L.; Dibden, J. W.; Owen, J. R.; Garcia-Araez, N. Impedance Characterization of the Transport Properties of Electrolytes Contained within Porous Electrodes and Separators Useful for Li-S Batteries. *J. Electrochem. Soc.* **2018**, *165*, A2741–A2749.

(39) Zhang, S.; Ueno, K.; Dokko, K.; Watanabe, M. Recent Advances in Electrolytes for Lithium-Sulfur Batteries. *Adv. Energy Mater.* **2015**, *5*, 1500117.

(40) Robba, A.; Vizintin, A.; Bitenc, J.; Mali, G.; Arčon, I.; Kavčič, M.; Žitnik, M.; Bučar, K.; Aquilanti, G.; Martineau-Corcus, C.; et al. Mechanistic Study of Magnesium–Sulfur Batteries. *Chem. Mater.* **2017**, *29*, 9555–9564.